ME 41 Engineering Design II Cold Forging Header Analysis

Stephanie Bentley, Rónán Gissler, Lawson Matthew

Introduction

The goal of this report is to analyze the components of a cold forging header machine and apply knowledge learned during the course to answer questions about this header. A cold forging header is a machine used to form the heads of fasteners without the addition of heat to reduce soften the material, enabling strain hardening to occur. As such, this machine needs to apply a large load to plastically deform the material in order to form the head on the fastener. Using a cold forging method instead of machining the fasteners will enhance their mechanical properties, specifically yield, ultimate, impact and fatigue strengths. For this analysis, the cold forging header was assumed to be a single die, two-blow header. The two blows consist of a preheading blow to form the approximate conical shape of the head and a final heading blow to fully form the shoulder head shape. In addition to the heading operation, the machine also performs accessory functions necessary to provide continuous automatic operation, like shearing the wire before heading.

A patented cold forging header (US2599053A), shown in Figure 1, was used as a model on which to base the analysis. Based on relative dimensions in the patent drawings, a SolidWorks assembly, displayed in Figure 2, was put together using a scale deemed reasonable by the course instructor, Professor Leisk. The parts and their associated dimensions in this assembly were then used throughout the analysis. Additionally, a research paper on tool stresses in cold heading of fasteners was used to determine the level of forces likely involved during the heading process [1].

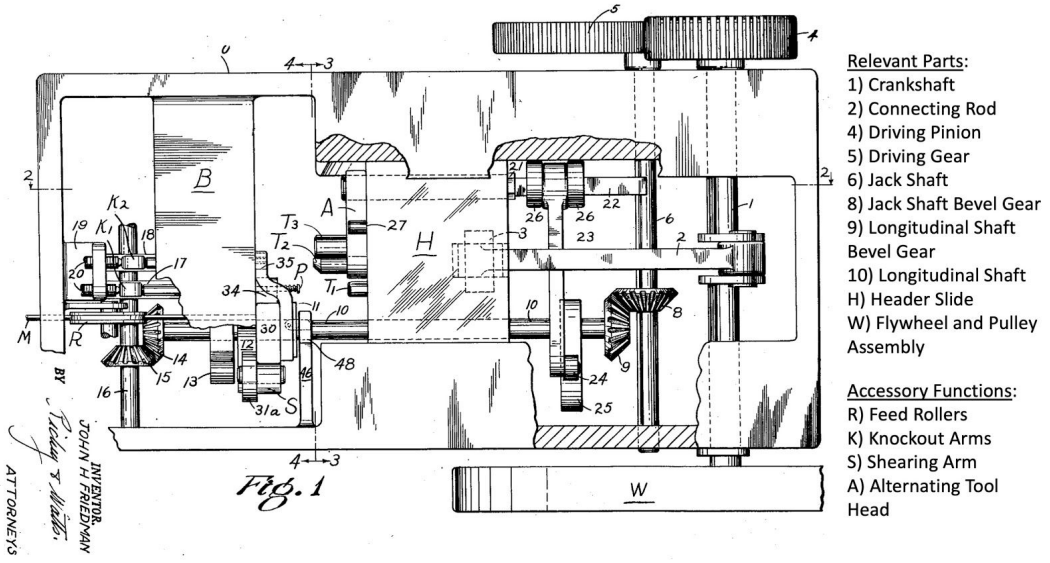

Figure 1. Patent Drawing of Cold Forging Header with Relevant Parts and Accessory Functions Labeled

This analysis does not examine every component of the cold forging header machine but instead focuses on the crankshaft, connecting rod, accessory gearing system, bearings used to support the crankshaft, and flywheel-motor system as labeled in Figure 1.

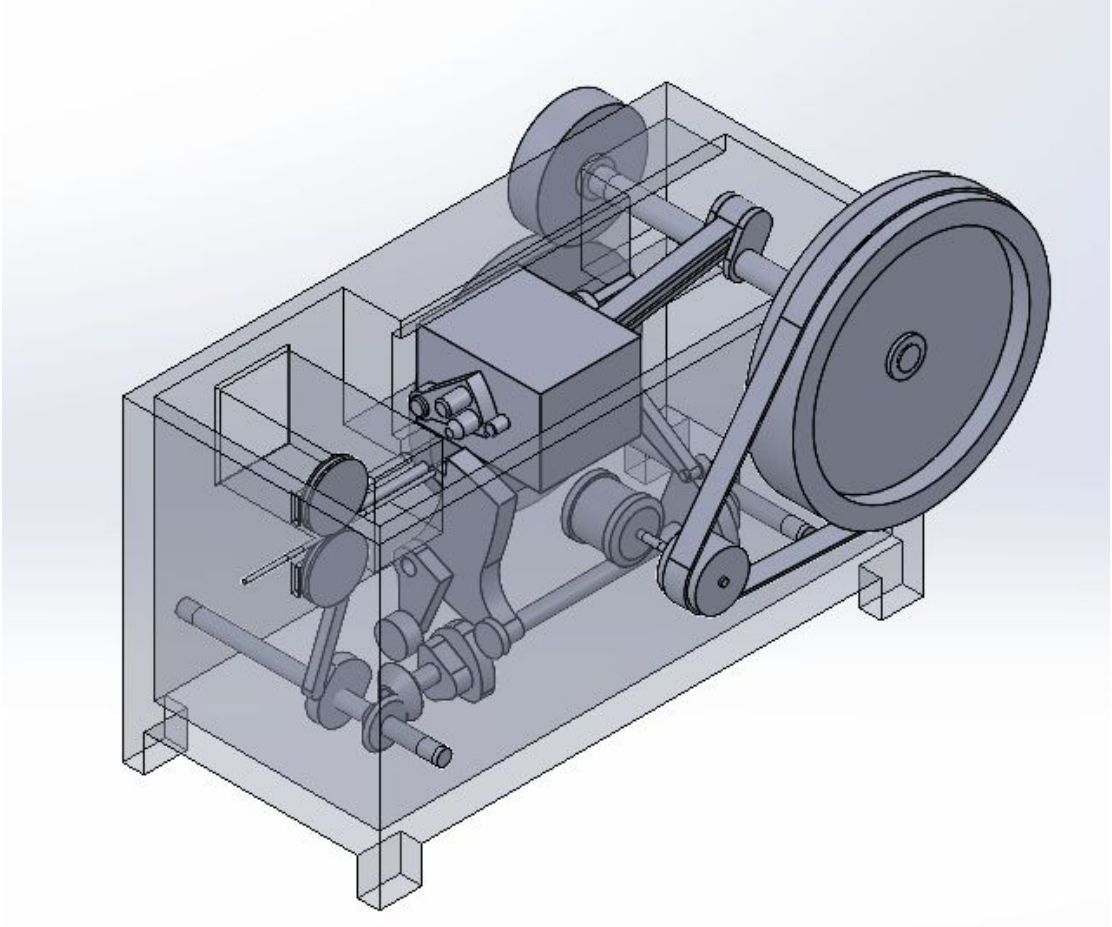

Figure 2. SolidWorks CAD Rendering of Cold Forging Header

Crankshaft Analysis

Three steps of analysis were conducted for the crankshaft. First, a free body diagram was drawn evaluating the relevant forces acting on the crankshaft during important moments in its rotation. Second, a finite element analysis (FEA) study was conducted in SolidWorks to determine the maximum deflection and stress experienced by the crankshaft. Third, an analytical approach was used to determine a factor of safety for the crankshaft in both static and fatigue failure. These steps illustrated considerations that may have arisen during the design of the crankshaft for the cold forging header to ensure the product functioned appropriately.

Using data from a research paper on cold heading of fasteners shown below in Figure 3, it was assumed that the peak force during preheading was 150 kN and the peak force during final heading was 600 kN throughout the crankshaft analysis.

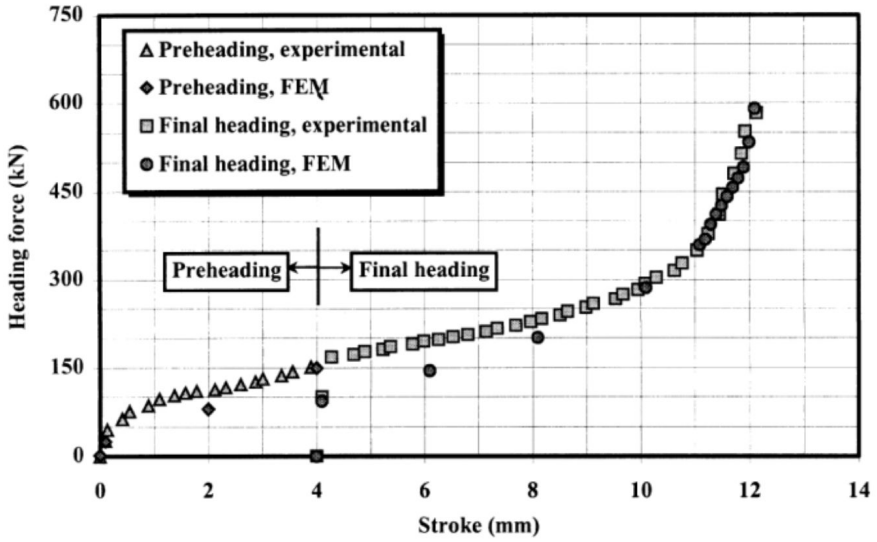

Figure 3. Heading Force versus Stroke Graph for Cold Heading of Fasteners [1]

Free Body Diagram

The external forces and torques acting on the crankshaft changed with time, so two important orientations during the heading cycle were chosen and two free body diagrams were drawn. The first shows the crankshaft orientation when the header slide is fully extended. The force acting on the crankshaft would be at a maximum and zero torque would be exerted on the crankshaft from the heading operation (Figure 3). The second shows the crankshaft orientation when the crankshaft starts to push the header slide forward, 90 degrees from max extension (Figure 4). The torque from the heading operation is assumed to be at a maximum here as the lever arm of the torque from the heading operation would be at a maximum. In reality this assumption of maximum torque is incorrect as the heading force causing the torque from the heading operation is smallest at this point. As the crankshaft rotates forward, the lever arm would

decrease while the heading force would increase, having countering effects on the magnitude of the torque from the heading operation.

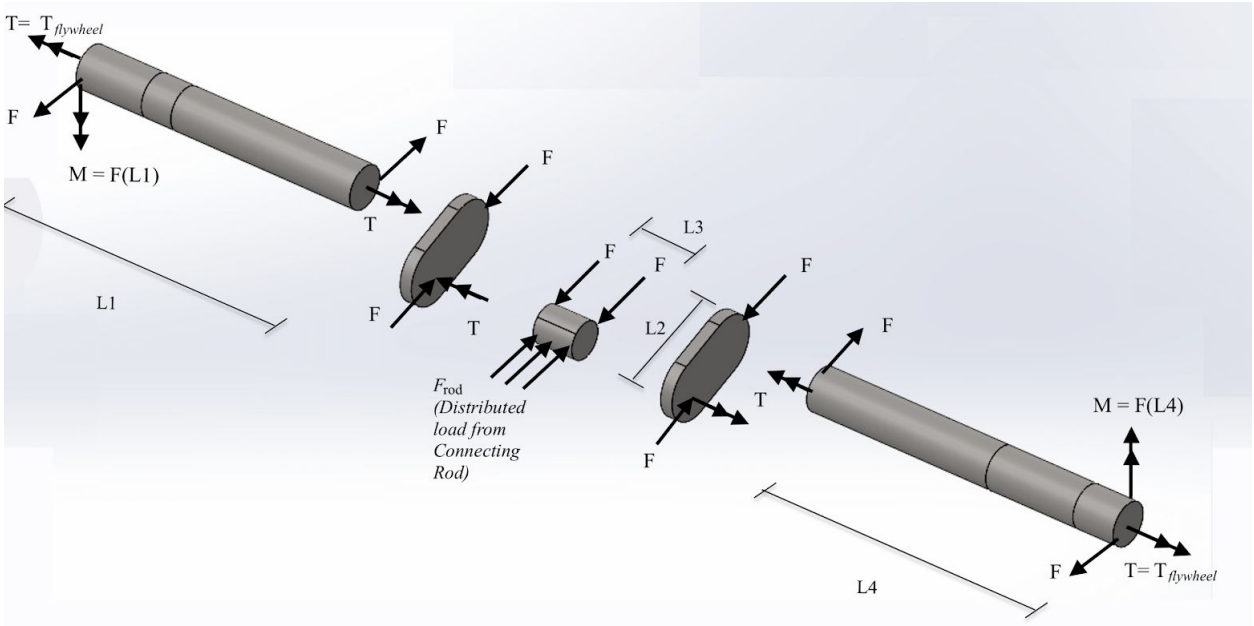

Figure 4. Free Body Diagram of Crankshaft at Max Force

L1	610.8 mm
L4	545.5 mm
Shaft Diameter	78.4 mm
L3	77.2 mm
F_{rod}	150 kN (preheading) 600 kN (final heading)
F	150/2 = 75 kN (preheading) 600/2 = 300 kN (final heading)
D	62.8 mm

Table 1. Legend for Free Body Diagrams

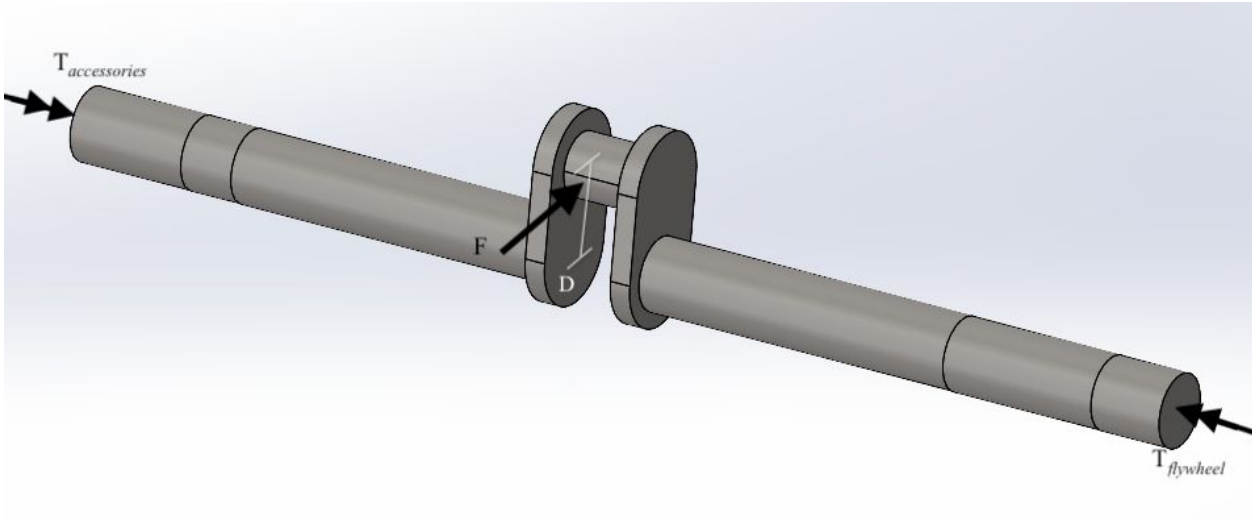

Figure 5. Free Body Diagram of Crankshaft at Max Torque

SolidWorks FEA

Given the significant forces involved in the heading operation, the crankshaft would experience substantial stress. Using Newton's 3rd Law, the force transferred to the workpiece during the heading process must also be experienced by the crankshaft causing it to deflect. Additionally, as the flywheel rotates the crankshaft is twisted to power the heading operation, creating a substantial amount of torsion on the crankshaft. Using FEA, the level of stress in the crankshaft can be predicted and areas of stress concentration identified. The maximum deflection of the crankshaft during the peak heading load can also be determined in order to consider when the positioning of the connecting rod and thus the heading slide may be affected by the deflection of the crankshaft. Additionally, the slope of the crankshaft during maximum deflection can be determined at the bearing supports located on the machine frame to evaluate whether bearing misalignment is a potential concern.

Using the crankshaft part included in the SolidWorks assembly, the FEA began with selecting an appropriate material for the crankshaft. Given the tremendous load required to perform the cold heading operation, the machine components require high strengths so as not to fail under these loads. Therefore, the expectation was that the machine was made from some form of tool steel. According to an article, popular tool steels used in industry include S7, D2, and A2 tool steels of which D2 tool steel is often used in cold forming dies [2]. Another source mentions that cold-work tool steels include "all diffused, high chromium class D, medium-alloy, air-hardening class A alloys, water hardening W alloys and oil-hardening O alloys. [3]" Looking

through tool steels of these class ratings on Matweb, most appeared to have a yield strength around 1500 MPa and an elastic modulus of about 200,000 MPa. Using this information, a material matching these requirements was selected from the SolidWorks materials library. Of the SolidWorks DIN Steel (Toolmaking) materials which had material properties near the requirements, the 1.2842 (90MnCrV8) material was selected given that it had the highest yield strength of the DIN Steel (Toolmaking) materials. The material had a yield strength of 1750 MPa, ultimate tensile strength of 1930 MPa, and an elastic modulus of 210,000 MPa.

Although the crankshaft part geometry appeared to be a faithful rendition of the patent drawing, 20 mm fillets were added inside the links on the center shaft where the connecting rod is mounted and 40 mm fillets were added outside the links on the shafts on either end. These fillets were added to reduce the impact of stress concentration on the FEA around the center links caused by the rapid change in part cross-section.

A static simulation was conducted in SolidWorks on the crankshaft part, with fixtures and loading conditions added to model the crankshaft's operation. A force of 600 kN, the peak force during final heading, was applied to the half-cylinder on the center shaft where the connecting rod was expected to make contact with the crankshaft. Full fixtures, limiting all rotation or translation, were added along the cylindrical ends of the shaft where the flywheel and spur gear would be mounted as these parts would move as one. Radial fixtures, limiting only translation in the plane perpendicular to the axis of the crankshaft, were applied on the shaft adjacent to the full fixtures, further in on the crankshaft. These radial fixtures represented where the crankshaft would sit inside the bore of the bearing supports, allowing the crankshaft to rotate freely while maintaining its position. Figure 6 depicts the loading conditions and fixtures in the crankshaft simulation.

With these boundary conditions in place, the simulation was ready for analysis. The part was broken apart using a relatively fine mesh with finer mesh control applied around the links where stress concentrations were expected to occur (Figure 6). Figures 7 and 8 display the result of the simulation.

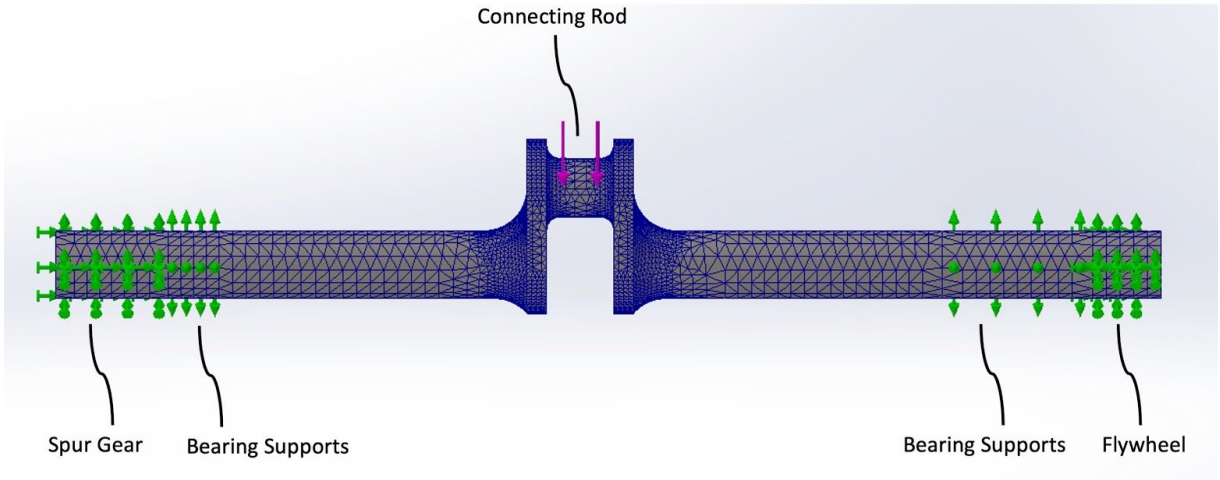

Figure 6. Mesh, Fixtures, and Loading Condition for Crankshaft

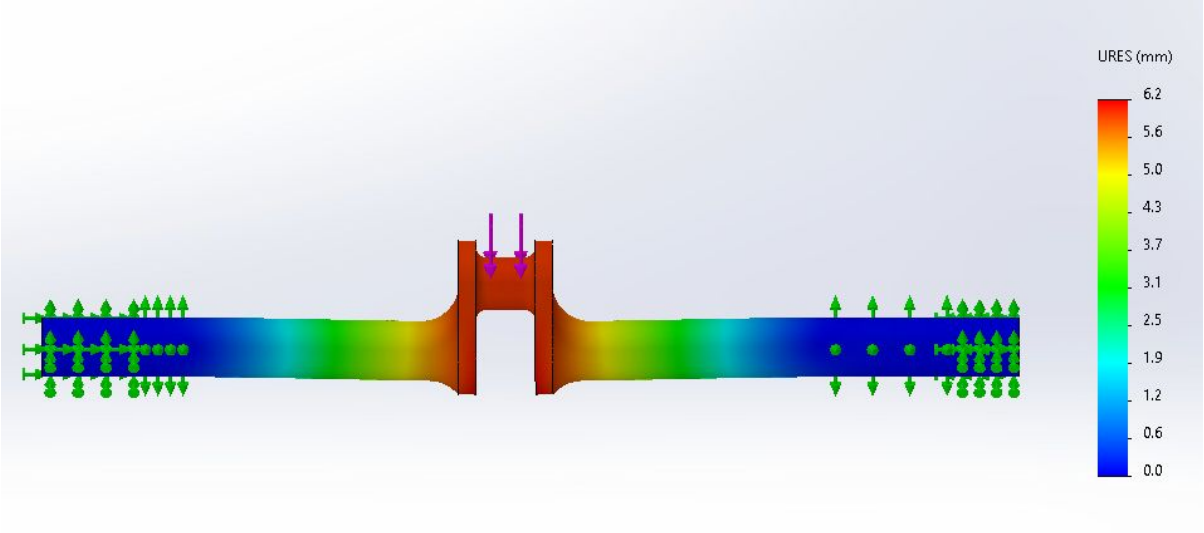

Figure 7. Deflection Plot of Crankshaft. The maximum deflection was 6.2 mm approximately in the center of where the load was applied from the connecting rod.

Examining Figure 7, the anticipated deflection of the crankshaft during heading seems significant, especially given the already small workpiece geometry. The true maximum deflection of the crankshaft would likely be less than 1 mm to ensure good contact between the workpiece and punch.

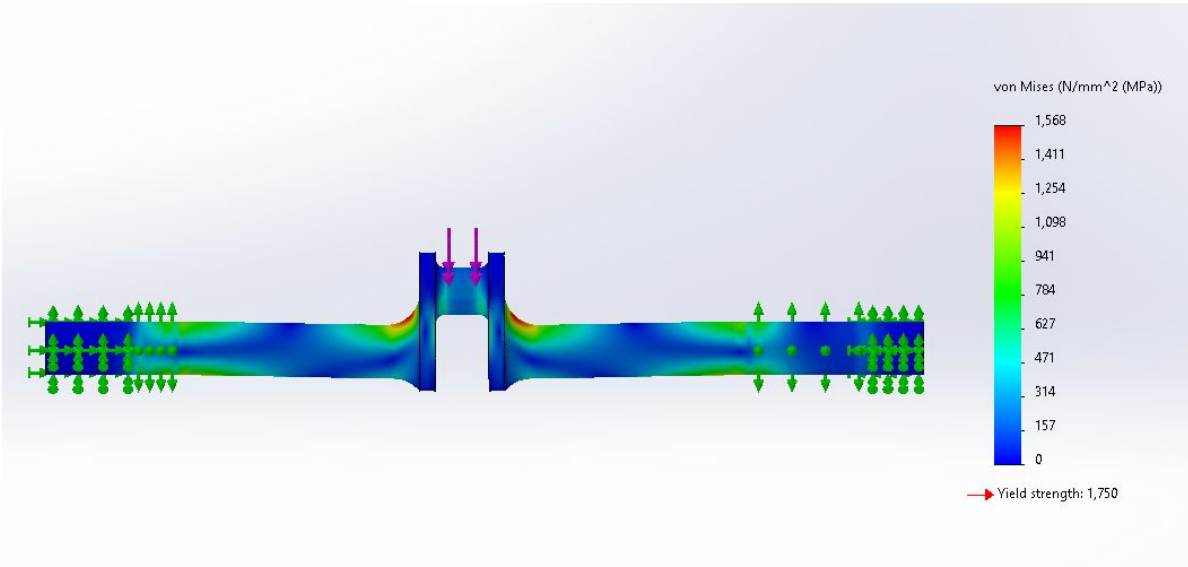

Figure 8. Stress Plot of Crankshaft. Note the stress concentrations adjacent to the central links and on either end of the shaft at the bearing supports.

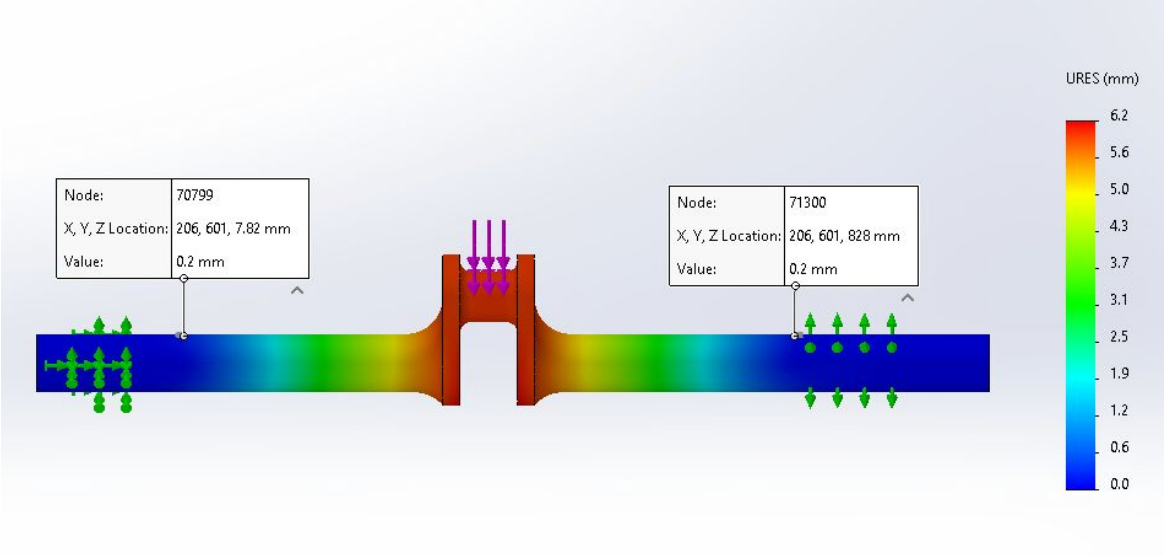

Figure 9. Slope Calculation of Crankshaft at Bearing Supports

The deflection was probed at a distance of 5 mm from the bearing supports at either end of the crankshaft and was found to be 0.2 mm as seen in Figure 9. Using trigonometry, the slope at the bearing supports can be found with those two distances.

$$tan() = \frac{0.2}{5} \Rightarrow = tan^{-1}(\frac{0.2}{5}) \approx 0.0340 \circ$$

Given the incredibly small slope angle of 0.0340° at the bearing supports, it is unlikely that the deflection of the crankshaft will cause any misalignment issues between the inner and outer races in each bearing.

Theoretical Failure Analysis

Introduction:

Of all the cold forging header machine components, the crankshaft was put through the most extreme loading conditions and thus it was most likely to fail. To evaluate the crankshaft's potential for failure, the first step was identifying the loading conditions the crankshaft would experience during heading operation. Examining the free-body diagram, the center shaft would experience normal stress in bending, transverse shear stress in bending, and direct shear stress at the connections to the links. The links would experience normal stress in bending, transverse shear stress in bending, and normal stress in compression. The shafts on either end would experience normal stress in bending, transverse shear stress in bending, and shear stress in torsion. Since all of these loading conditions would make for quite a complicated analysis, only a few were selected with the expectation that they would be the most significant contributors to crankshaft failure. The key loading conditions are likely the normal stress in bending and shear

stress in torsion on the long shafts on either end of the crankshaft. The normal stress in bending was selected given the large moment that would develop outwards in both directions due to the force applied by the connecting rod. The shear stress in torsion was selected given the torque on the shaft from the flywheel and was therefore expected to be significant.

Choosing a specific instant in the crankshaft's rotation, the force that contributes to the normal stress in bending can be solved for using the free body diagram given the known heading force. The torque that contributes to the shear stress in torsion however cannot be easily determined by looking at the free body diagram. Instead a work-energy approach was used to determine the average torque required for each step of the heading operation during one full rotation of the crankshaft.

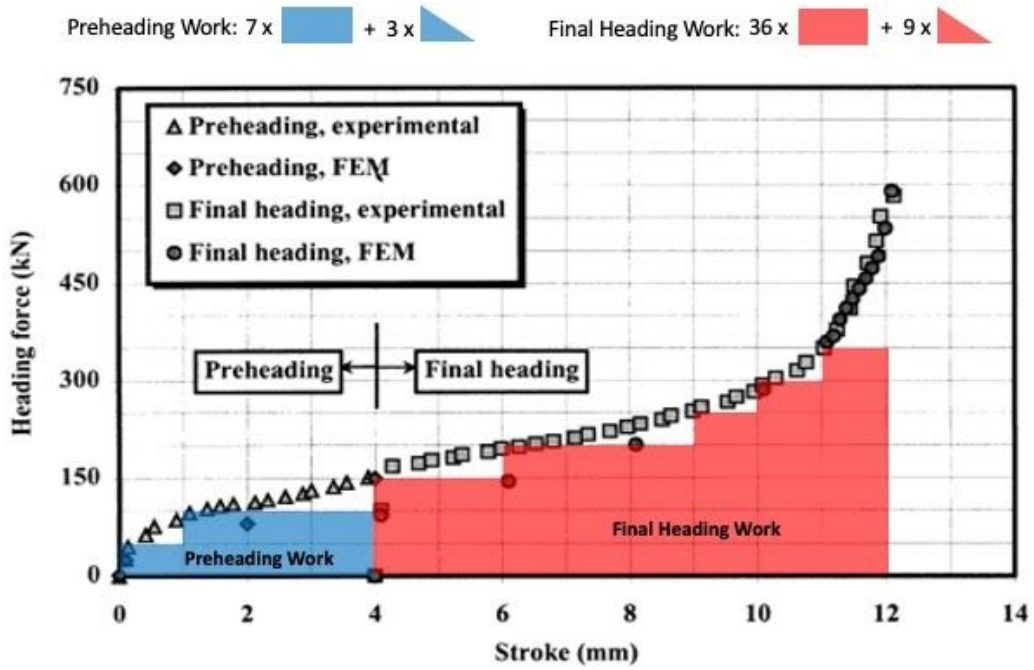

Figure 10. Work-Energy Approach to Solve for Crankshaft Torque. Integrating the heading force with respect to stroke, the amount of work required for heading was determined. Had the data for this plot been provided, a more legitimate integral would have been calculated.

The preheading and final heading work were calculated by finding the area under the curve pictured above in Figure 10.

$$\text{Preheading Work: } W = 7 \times (50 \times 1) + 3 \times \frac{(50 \times 1)}{2} = 350 + 75 = 425\ N \cdot m$$

$$\text{Final Heading Work: } W = 36 \times (50 \times 1) + 9 \times \frac{(50 \times 1)}{2} = 1800 + 225 = 2025\ N \cdot m$$

Assuming there are no energy losses in the machine, the work done in the heading operation itself must also be equal to the work done to rotate the crankshaft to perform the heading operation. To determine the average torque required for heading over one rotation of the

crankshaft, the work done for each step of the heading operation was simply divided by 2π, the measure of a full rotation in radians.

$$\text{Average Torque Over Preheading: } T = \frac{425\ N \cdot m}{2\pi} \approx 67.6\ N \cdot m$$
$$\text{Average Torque Over Final heading: } T = \frac{2025\ N \cdot m}{2\pi} \approx 322\ N \cdot m$$

These torque values represent the average torque required for the heading operation, but they do not represent the average torque of the flywheel on the crankshaft. The torque required from the flywheel is the sum of the torque required for heading and the torque required to execute the accessory functions of the machine. For this fatigue analysis, only the torque required to execute the heading operation was considered as it was anticipated to be more significant than the torque required to execute the accessory functions.

Even though the average torque during each heading step has been determined, the maximum torque is of greater interest when considering failure. To determine the maximum torque, assumptions need to be made regarding how the force and torque on the crankshaft change with time. As a result, understanding how the normal stress in bending and shear stress in torsion on the crankshaft change with time will be useful during the fatigue failure analysis.

To begin, the force on the crankshaft and therefore also the normal stress in bending of the crankshaft can be visualized as two separate constant amplitude sinusoidal curves. These curves, plotted below in Figure 11, represent the repeated loading for each operation, from 0 to 150 kN of force for preheading and from 0 to 600 kN of force for final heading. Since preheading and final heading occur during alternating rotations of the crankshaft, they are shown out of phase with one another. Stacking these two curves into a single curve, the fluctuating force and normal stress in bending on the crankshaft over the course of heading operation can be determined.

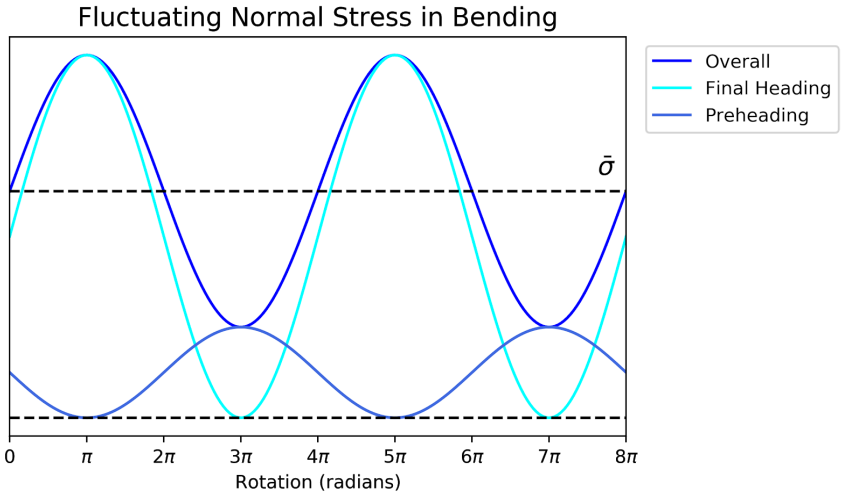

Figure 11. Model for Fluctuating Normal Stress in Bending on Crankshaft

Using the model pictured above in Figure 11, the average force on the crankshaft can be calculated by adding half the peak force during final heading and half the peak force during preheading, equivalent to the average peak heading force.

$$F_{avg} = (600/2) + (150/2) = 300 + 75 = 375\ kN$$

The shear stress in torsion can be approximated in a similar manner. As indicated in the free-body diagram, the torque lever arm produced by the links on the crankshaft is greatest 90 degrees before full extension of the header slide. This is not necessarily indicative of greatest torque as the force increases as the lever arm decreases when the header slide extends, but for this analysis we will assume that the torque is indeed at a maximum when the crankshaft is 90 degrees from extension. Therefore, the torque on the crankshaft would be 90 degrees or $\frac{\pi}{2}$ radians out of phase with the force on the crankshaft.

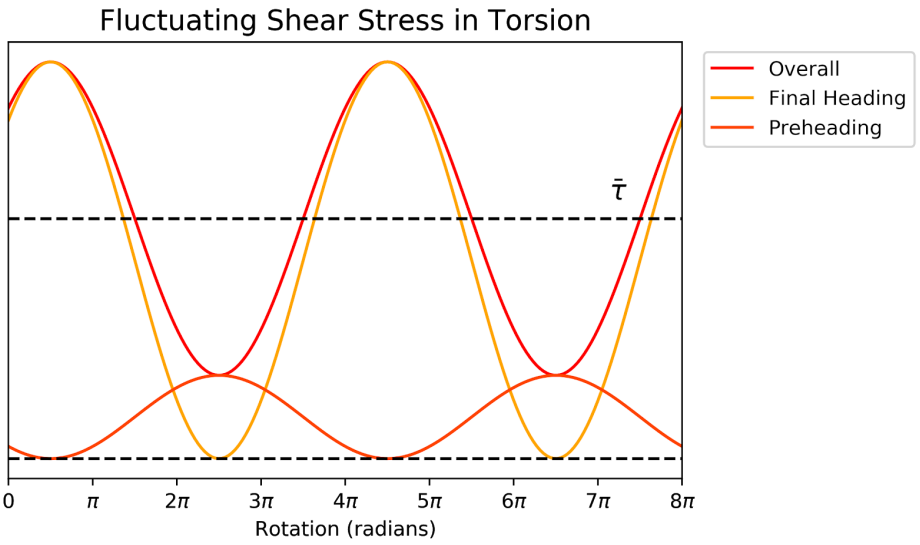

Figure 12. Model for Fluctuating Shear Stress in Torsion on Crankshaft

Using the model picture above in Figure 12, the maximum torque can be calculated by simply using the peak value expected from the final heading curve, which would just be two times the average torque from final heading.

$$T_{max} = 2 * 322\ N \cdot m = 644\ N \cdot m$$

Plotting the overall normal stress in bending and overall shear stress in torsion together, an image of the fluctuating loads most likely to result in crankshaft failure is produced below in Figure 13. The normal stress in bending is expected to have greater magnitude than shear stress in torsion as the moment increases along the shaft outwards from where the load is applied while the torque is constant on either end of the crankshaft at any one moment.

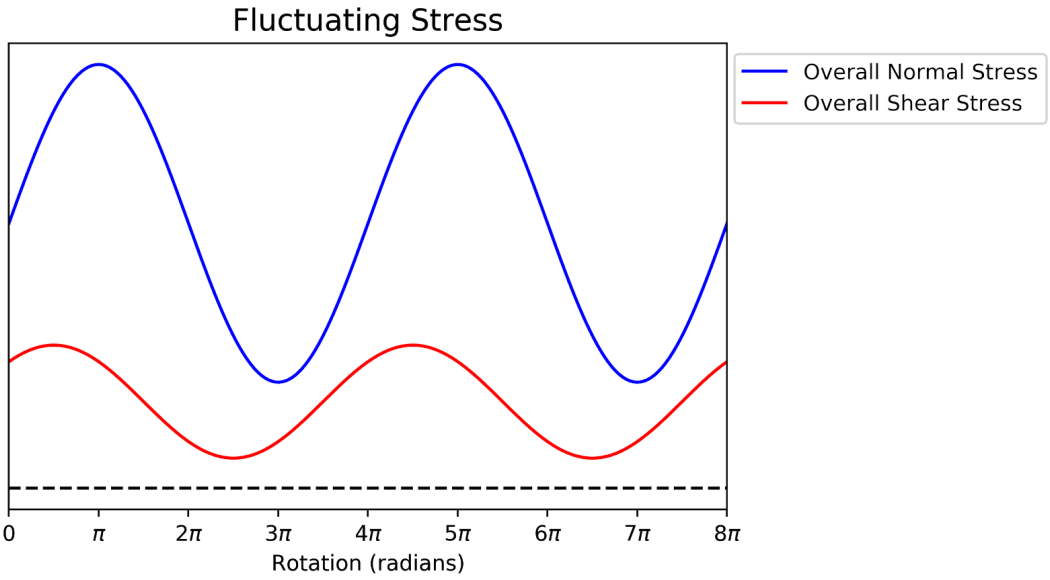

Figure 13. Model for Overall Fluctuating Stress on Crankshaft

Static Failure Analysis:

Having described the loading the crankshaft will experience, a factor of safety guarding against static failure of the crankshaft can now be calculated. Through FEA, the edges of the central links and the ends of the crankshaft at the bearing supports were identified as potential areas of high stress. Given that the stress concentrations at the central links were substantially reduced in the FEA just by adding fillets around the links, the stress concentrations there were assumed to be less difficult to design for. On the other hand, the bending moment is at a maximum at either end of the shaft and therefore the stress in those locations is a more serious concern. Using this reasoning, a stress element was selected for the failure analysis at the slightly longer end of the crankshaft shown below in Figure 14.

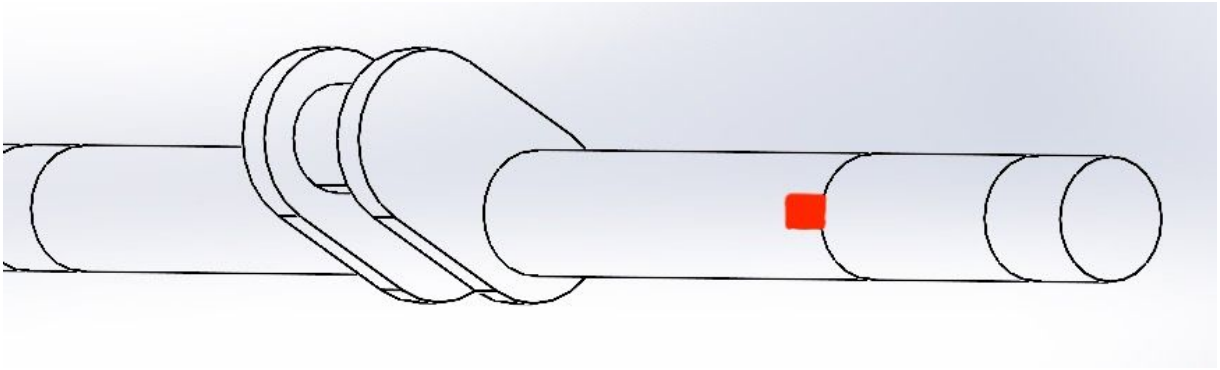

Figure 14. Critical Stress Element on Crankshaft

As was mentioned earlier, the primary loading conditions that are evaluated along the crankshaft are the normal stress in bending and shear stress in torsion. The maximum value for these two stresses was then calculated for use in the static failure analysis. The force used to calculate the maximum normal stress in bending was the maximum reaction force that occurred during the final heading step. The torque used to calculate the maximum shear stress in bending was the maximum torque T_{max} that occurred just prior to the final heading step, derived using the model for fluctuating shear stress in torsion on the crankshaft.

$$\sigma_{bending} = \frac{Mc}{I} = \frac{FL\,(d/2)}{I} = \frac{300\times10^{3}\,N * 0.357\,m * (0.0784/2\,m)}{\pi * (0.0784\,m)^{4} * 1/64} \approx 2264\,MPa$$

$$\tau_{torsion} = \frac{Tr}{J} = \frac{644\,N{\cdot}m * (0.0784/2\,m)}{\pi * (0.0784\,m)^{4} * 1/32} \approx 6.81\,MPa$$

Based on this calculation, the shear stress in torsion appears to be negligible in comparison with the normal stress in bending. This is a surprising result given that the torque on the crankshaft is ultimately what is providing the heading force. For the critical stress element selected, normal stress in bending would cause compression of the element along the axis of the crankshaft and shear stress in torsion would cause twisting of the element in the direction of crankshaft rotation. A magnified view of the stress element is shown below in Figure 15, simplified to just a plane stress element.

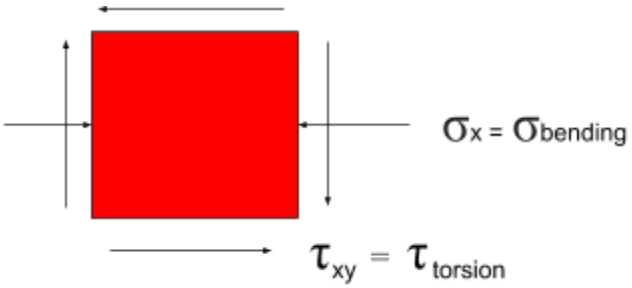

Figure 15. Labeled Plane Stress Element

Using Distortion-Energy Theory, a factor of safety guarding against static failure is calculated below using von Mises stress.

$$\sigma' = (\sigma_x^{\,2} - \sigma_x\sigma_y + \sigma_y^{\,2} + 3\tau_{xy}^{\,2})^{1/2} = (2264^{\,2} - 0 + 0 + 3(6.81)^2)^{1/2} \approx 2264\,MPa$$

$$n = S_y / \sigma' = \frac{1750\,MPa}{2264\,MPa} \approx 0.773$$

The factor of safety computed is less than 1 indicating that yielding occurs at this element on the crankshaft. This would not be the case in the real product as this would likely soon lead to product failure even if the steel did initially benefit from some strain strengthening. Instead it is likely that the model used for analysis is not a faithful representation of the true cold forging header machine. The material selected for the crankshaft analysis may not be strong enough or the diameter selected for the crankshaft may be too narrow. However, this would not explain

why then the FEA model which makes use of the same assumptions does not show yielding at that same location and in fact shows a stress level well below the yield level of the material.

Fatigue Failure Analysis:

If the crankshaft already has a factor of safety less than one in static failure, the factor of safety will be even smaller in fatigue failure. The heading machine is expected to operate at a fast pace for hours a day over the course of many years. Throughout the course of its operation, the stresses in the crankshaft fluctuate significantly making it susceptible to fatigue failure over time. To determine a factor of safety guarding against fatigue failure of the crankshaft the Stress-Life approach is used.

Using the models for fluctuating normal stress in bending and fluctuating shear stress in torsion from Figures 11 and 12 respectively, the alternating and mean stresses for normal stress and shear stress can be determined.

$$\sigma_{m,\,bending} = \frac{Mc}{I} = \frac{F_{avg}L\,(d/2)}{I} = \frac{375\times10^3\,N * 0.357\,m * (0.0784/2\,m)}{\pi * (0.0784\,m)^4 * 1/64} \approx 2.83\times10^3\,MPa$$

$$\sigma_{a,\,bending} = \frac{Mc}{I} = \frac{F_{a}L\,(d/2)}{I} = \frac{225\times10^3\,N * 0.357\,m * (0.0784/2\,m)}{\pi * (0.0784\,m)^4 * 1/64} \approx 1.70\times10^3\,MPa$$

$$\tau_{m,\,torsion} = \frac{T_{avg}r}{J} = \frac{322\,N{\cdot}m * (0.0784/2\,m)}{\pi * (0.0784\,m)^4 * 1/32} \approx 3.40\,MPa$$

$$\tau_{a,\,torsion} = \frac{T_{a}r}{J} = \frac{322\,N{\cdot}m * (0.0784/2\,m)}{\pi * (0.0784\,m)^4 * 1/32} \approx 3.40\,MPa$$

Instead of using two separate alternating and mean stresses, the expressions above can be rewritten as a single set of alternating and mean stresses using von Mises stress.

$$\sigma_m' = [(\sigma_{m,\,bending})^2 + 3(\tau_{m,\,torsion})^2]^{1/2} = [(2.83\times10^3)^2 + 3(3.40)^2]^{1/2} \approx 2.83\times10^3\,MPa$$

$$\sigma_a' = [(\sigma_{a,\,bending})^2 + 3(\tau_{a,\,torsion})^2]^{1/2} = [(1.70\times10^3)^2 + 3(3.40)^2]^{1/2} \approx 1.70\times10^3\,MPa$$

As was also seen in the static failure analysis, the shear stress in torsion is negligible compared to the normal stress in bending. The cold header machine was expected to operate for 260 days a year at 6 hours a day producing 175 parts/min (350 RPM). From this information the number of stress cycles on the crankshaft can be calculated.

$$N = (350\,RPM) \times \frac{60\,mins}{1\,hour} \times \frac{6\,hours}{1\,day} \times \frac{260\,days}{1\,year} \times 50\,years = 1.638\times10^9\,cycles$$

Since this number of cycles is greater than the 1 million cycles used to determine the endurance stress limit below which the part is expected to have infinite life, the endurance limit is used to calculate the factor of safety. The endurance limit of the crankshaft is calculated with the Stress-Life approach, which determines the endurance limit based on empirical data from R. R. Moore tests, constant amplitude loading tests of carefully controlled test specimens. This theory is employed with the help of expressions provided in *Shigley's Mechanical Engineering Design* textbook and will be referenced as *Shigley's* going forward. Using the ultimate strength

of the crankshaft material, the endurance limit can be estimated using expression 6-8 from *Shigley's*.

$$S_e' = 700\ MPa\ since\ S_{ut} > 1400\ MPa$$

Since the setup of the crankshaft differs from that of the R. R. Moore tests, corrections must be made to the endurance limit to account for these differences using Marin factors. Using *Shigley's*, five Marin factors are considered: surface factor, size factor, load factor, temperature factor, and reliability factor.

Given the unique geometry of the part and the tight tolerances required at the links where the connecting rod is mounted, the part is likely machined. A surface factor can then be calculated using Table 6-2 from *Shigley's*.

$$k_a = 4.51 \times S_{ut}^{-0.265} = 4.51 \times (1930\ MPa)^{-0.265} \approx 0.607$$

To account for the diameter of the rotating crankshaft loaded in bending and torsion, expression 6-20 from *Shigley's* is used to calculate the size factor.

$$k_b = 1.51 d^{-0.157} = 1.51 \times (78.4\ mm)^{-0.157} \approx 0.761\ since\ 51 < d = 78.4 < 254\ mm$$

The crankshaft is loaded in both bending and torsion, so the load factor would simply be $k_c = 1$ and thus plays no role in this analysis.

The cold forging header machine is expected to operate at room temperature conditions at which the material properties were recorded, so no temperature factor was used (i.e. $k_d = 1$).

To ensure that the crankshaft, arguably the most important part in the cold forging header machine, has a reliability of 90%, a reliability factor of $k_e = 0.897$ is taken from Table 6-5 of *Shigley's*.

Combining these Marin factors together, the test endurance limit can be translated into a corrected endurance limit.

$$S_e = k_a k_b k_c k_d k_e S_e' = (0.607)(0.761)(1)(1)(0.897)(700\ MPa) \approx 290\ MPa$$

To calculate a factor of safety for the fatigue failure of the crankshaft, the simple and conservative Goodman Line method was used.

$$n_f = \left[\frac{\sigma_a'}{S_e} + \frac{\sigma_m'}{S_{ut}}\right]^{-1} = \left[\frac{1.70 \times 10^3 MPa}{290\ MPa} + \frac{2.83 \times 10^3 MPa}{1930\ MPa}\right]^{-1} \approx 0.136$$

Given that the crankshaft was already found to be yielding under static loading conditions, it comes as no surprise that the factor of safety in fatigue is so much smaller than one.

Connecting Rod Buckling Analysis

The rotation of the crankshaft is translated into the linear motion of the heading slide by the connecting rod, driving the attached punches for the pre-heading and final heading strokes. Through this motion the crankshaft exerts significant force axially on the connecting rod which is then exerted on the workpiece through the punch. However, since the connecting rod must be a long, slender member to translate the rotational motion of the crankshaft into the linear motion of the punch, the connecting rod may be at risk of buckling under the significant axial loads. To determine the functionality and safety of the machine, the factor of safety guarding against buckling of the connecting rod is calculated. Additionally, another factor of safety guarding against buckling of the connecting rod is calculated considering a 50% reduced cross-sectional area. This illustrates the sensitivity of the connecting rod buckling failure to reductions in cross section had other design restrictions made a thinner connecting rod necessary.

To analyze the buckling of the connecting rod, dimensions from the SolidWorks part were used as a model. The rod is a rectangular prism with hoops on either end to interface with the crankshaft and heading slide. The prism also features rectangular indentions on the side faces, creating a shape resembling an I-beam. The connecting rod was approximated as an I-beam for this analysis since the regions of the rod that do not have this I-beam cross-section have larger cross-sections and are thus less susceptible to buckling. Therefore, this analysis focused on the length with the greatest propensity to buckle, which was the length of the cross-section resembling the I-beam, ignoring the regions on either end. Thus, it was assumed that $l = 526.7mm$. The connecting rod geometry is shown below in Figure 16.

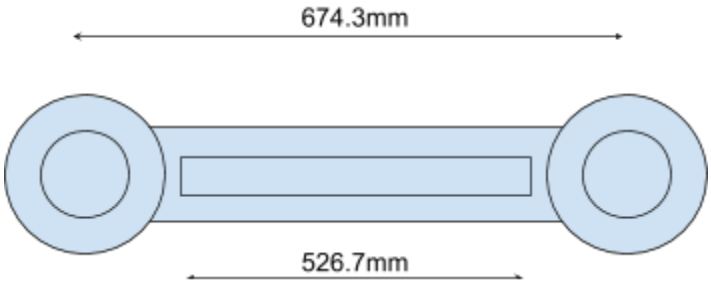

Figure 16. Side View of Connecting Rod Geometry Indicating Total Length and Length Used for Buckling Analysis

It was assumed that the connecting rod was made of the same material as the crankshaft, since the connecting rod experiences similarly significant loads and thus has similar strength requirements. The material properties used included an elastic modulus of $E = 2.1 * 10^{11} Pa$ and yield strength of $S_y = 1750MPa$.

The dimensions for the I-beam approximation of the connecting rod were measured from the SolidWorks part, and are shown below in Figure 17.

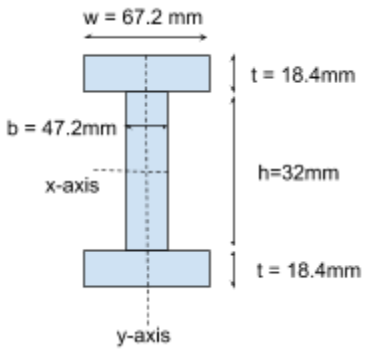

Figure 17. Approximated I-beam Cross-section of Connecting Rod with Dimensions

The cross-sectional area of this I-beam is:

$$A = 2 * w * t + b * h = 2 * 0.0672m * 0.0184m + 0.0472m * 0.032m = 0.00398m^2$$

The I-beam can either buckle around the x-axis or the y-axis, indicated above in Figure 17. Both moments of inertia are calculated to determine about which axis the connecting rod is more susceptible to buckling failure.

$$I_{yy} = \frac{b^3 * h}{12} + 2 * (\frac{w^3 * t}{12}) = \frac{(0.0472\ m)^3 * 0.032\ m}{12} + 2 * (\frac{(0.0672\ m)^3 * 0.0184\ m}{12}) = 1.211 * 10^{-6}\ m^4$$

$$I_{xx} = \frac{h^3 * b}{12} + 2 * (\frac{t^3 * w}{12} + w * t * (\frac{t+h}{2})^2)$$

$$= \frac{(0.032\ m)^3 * 0.0472\ m}{12} + 2 * (\frac{(0.0184\ m)^3 * 0.0672\ m}{12}) + 0.0672\ m * 0.0184\ m * (\frac{0.0184\ m + 0.032\ m}{2})^2) = 1.769 * 10^{-6}\ m^4$$

Since the buckling length and cross-sectional area of the rod is the same regardless of which axis the beam buckles around, a smaller moment of inertia will produce a smaller radius of gyration and a larger slenderness ratio. At a larger slenderness ratio the rod will buckle under a smaller critical load. Since the moment of inertia around the y-axis is smaller than that around the x-axis, the connecting rod is more likely to buckle around the y-axis at a smaller load. Therefore, the value for moment of inertia around the y-axis is used to calculate the critical load under which buckling failure will occur. This critical load depends on the radius of gyration and slenderness ratio as calculated below.

$$\text{Radius of gyration: } k = \sqrt{\frac{I_{yy}}{A}} = \sqrt{\frac{1.211 * 10^{-6}\ m^4}{0.00398\ m^2}} = 0.0174\ m$$

$$\text{Slenderness ratio: } \frac{l}{k} = \frac{0.5267\ m}{0.0174\ m} = 30.27$$

Both ends of the connecting rod are modeled as round hoops that fit around the crankshaft and a mechanism inside the heading slide. Since these ends can rotate freely around the shaft but resist rotation in other directions and displacement in all directions (assuming the rod cannot slide along the other members), the end conditions for the connecting rod are assumed

to both be pivots for which the end condition constant is $C = 1$ using Table 4-2 from *Shigley's*. With this end constant and the material properties described above, the critical slenderness ratio was calculated.

$$\text{Critical slenderness ratio: } \left(\frac{l}{k}\right)_1 = \left(\frac{2*\pi^2*C*E}{S_y}\right)^{1/2} = \left(\frac{2*\pi^2*1*2.1*10^{11}\,Pa}{1.75*10^9\,Pa}\right)^{1/2} = 48.67$$

Since the critical slenderness ratio is greater than the slenderness ratio calculated for the connecting rod buckling about the y-axis ($48.67 > 30.27$), the J. B. Johnson equation more accurately represents the member's propensity for buckling than the Euler equation. Using the J. B. Johnson equation, the critical load at which buckling failure of the connecting rod is expected to occur is calculated.

$$P_{Cr} = A*\left[S_y - \left(\frac{S_y}{2\pi}*\frac{l}{k}\right)^2 * \frac{1}{C*E}\right] =$$
$$0.00398\,m^2 * \left[1.75*10^9\,Pa - \left(\frac{1.75*10^9\,Pa}{2\pi}*30.27\right)^2 * \frac{1}{1*2.1*10^{11}\,Pa}\right] = 5618\,kN$$

The maximum force applied on the connecting rod during heading operation is the maximum force of the final heading stroke, 600 kN, which is axially loaded on the connecting rod. The factor of safety for the connecting rod in buckling is the ratio then of the critical load to this maximum force.

$$\text{Factor of Safety: } n = \frac{P_{Cr}}{F} = \frac{5618kN}{600kN} = 9.36$$

This factor of safety guarding against buckling of the connecting rod is significantly greater than one, indicating that the connecting rod is not at risk of buckling during the operation of the machine.

Reduced Cross-Section Buckling Analysis

If instead it is now assumed that the area of the connecting rod cross-section is reduced by 50%, a new factor of safety guarding against buckling can be calculated. This reduction does not affect the approximation of the cross-section as an I-beam or the length of the member $l = 526.7mm$, as shown below in Figure 18.

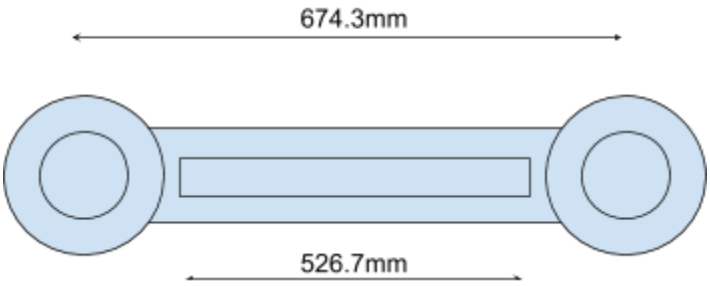

Figure 18. Side View of Connecting Rod Geometry Indicating No Changes when Cross-section is Reduced.

To reduce the cross-sectional area by 50%, there are many ways to scale down the geometry. However, to isolate the effect of changing the cross-sectional area as much as possible from changing the distribution of mass, each dimension was scaled down proportionally by $\sqrt{2}$. The updated cross-section dimensions are shown below in Figure 19.

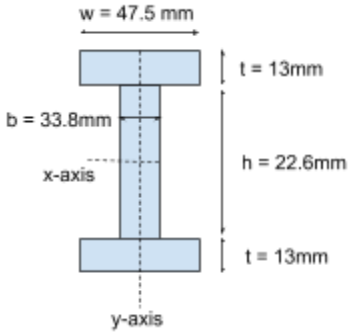

Figure 19. I-beam Cross-section of Connecting Rod with Dimensions from 50% Reduction in Area

The updated cross-sectional area was calculated, confirming that the cross-sectional area had been reduced by 50%.

$$A = 2 * w * t + b * h = 2 * 0.0475\ m * 0.013\ m + 0.0338\ m * 0.0226\ m = 0.0020 m^2$$

Since the ratio of dimensions did not change, the more vulnerable axis is not expected to change, and both moments of inertia were calculated again to confirm that the connecting rod is still most vulnerable to buckling around the y-axis.

$$I_{yy} = \frac{b^3 * h}{12} + 2 * (\frac{w^3 * t}{12}) = \frac{(0.0338m)^3 * 0.0226m}{12} + 2 * (\frac{(0.0475m)^3 * 0.013m}{12}) = 3.04 * 10^{-7} m^4$$

$$I_{xx} = \frac{h^3 * b}{12} + 2 * (\frac{t^3 * w}{12} + w * t * (\frac{t+h}{2})^2)$$

$$= \frac{0.0226^3 * 0.0338}{12} + 2 * (\frac{0.013^3 * 0.0475m}{12} + 0.0475m * 0.013m * (\frac{0.013m + 0.0226m}{2})^2) = 4.41 * 10^{-7} m^4$$

Using the moment of inertia about the y-axis, the radius of gyration and slenderness ratio were calculated.

$$\text{Radius of gyration: } k = \sqrt{\frac{I_{yy}}{A}} = \sqrt{\frac{3.04*10^{-7}\ m^4}{0.002\ m^2}} = 0.0149\ m$$

$$\text{Slenderness ratio: } \frac{l}{k} = \frac{0.5267\ m}{0.0149\ m} = 35.46$$

Since there is no change in the material properties or end constant, the critical slenderness ratio also remains unchanged.

$$\text{Critical slenderness ratio: } \left(\frac{l}{k}\right)_1 = \left(\frac{2*\pi^2*C*E}{S_y}\right)^{1/2} = \left(\frac{2*\pi^2*1*2.1*10^{11}\ Pa}{1.75*10^9\ Pa}\right)^{1/2} = 48.67$$

Since the critical slenderness ratio is again greater than the slenderness ratio $(48.67 > 35.46)$, the J. B. Johnson equation more accurately represents the member's propensity for buckling than the Euler equation. Using the J. B. Johnson equation, the critical load at which buckling failure of the connecting rod is expected to occur is calculated.

$$P_{Cr} = A*[S_y - (\frac{S_y}{2\pi} * \frac{l}{k})^2 * \frac{1}{C*E}] =$$
$$0.002*[1.75*10^9\ Pa - (\frac{1.75*10^9\ Pa}{2\pi} * 35.46)^2 * \frac{1}{1*2.1*10^{11}\ Pa}] = 2571\ kN$$

Assuming the connecting rod experiences the same magnitude of force at the reduced cross-section, the factor of safety of the connecting rod is again calculated based on the maximum force of the final heading, 600 kN.

$$\text{Factor of safety: } n = \frac{P_{Cr}}{F} = \frac{2571kN}{600kN} = 4.28$$

Since the factor of safety is still greater than 1, the connecting rod is not vulnerable to buckling even if the cross-sectional area were to be reduced by 50%. This calculation indicates that the cross-section of the connecting rod could be adjusted in response to other design constraints without significantly increasing the risk of buckling failure.

Accessory Function Gearing System Analysis

The main mechanism of the machine is to plastically deform the workpiece into the desired shape, which is driven by the rotation of the crankshaft being translated into the linear motion of the punches through the connecting rod. However, in order to continuously and automatically apply the two blows, other secondary systems work to draw in in the wire stock and shear it, position the workpiece between the punch and the die, switch between the pre-heading and final heading punches, and finally knock out the finished piece before the process repeats. While these secondary systems are not expected to require the same magnitude of force that the heading blows themselves do, the forces they require are still non-negligible.

To operate the secondary systems in sync with the heading operation, they are driven from the crankshaft through a series of gears that translate the rotational speeds and torques from the crankshaft into those appropriate for these systems. At the opposite end of the crankshaft from the flywheel, the crankshaft is fixed to the driving pinion with a diameter of 408 mm in the SolidWorks model. Thus, the driving pinion and the crankshaft rotate together at the same speed. The driving pinion meshes with a larger driving gear with a diameter of 784 mm in the SolidWorks model. The pinion drives the gear, transmitting an increased output torque and a decreased output rotational speed. Since the cold forging header machine is expected to produce 175 parts/min and two full revolutions of the crankshaft are required for each part, the crankshaft would rotate at 350 RPM. Using the ratio of gear diameters, the rotational speed of the driving gear can be calculated.

$$\frac{d_A}{d_B} = \frac{n_B}{n_A} = \frac{T_A}{T_B}$$

$$n_g = \frac{d_p}{d_g} * n_p = \frac{408\ mm}{784\ mm} * 350\ RPM\ = 182\ RPM$$

The jack shaft is fixed to the driving gear and a bevel gear is fixed further along the length of the jackshaft, so all components rotate together at the same speed of 182RPM. The jack shaft bevel gear meshes with a bevel gear on the longitudinal shaft. Since both bevel gears have an outer diameter of 165mm, these gears change the direction of rotation rather than the speed or torque. Thus, the bevel gears and their corresponding shaft rotate at the same rotational speed. The bevel gears function to translate rotation to a perpendicular axis running the length of the cold forging header machine to drive the secondary systems located further up on the machine. From the longitudinal shaft, all the secondary systems are driven.

The torque required by all of the accessories is likely dominated by the force needed to shear the workpiece material. Since the workpiece is expected to be made of DIN37Cr4 (AISI 5135 steel), it has a shear strength of $S = 320\ MPa$ [5]. The diameter of the workpiece before it is sheared is 9mm, which represents both the thickness of the material and the length of the cut edge. Using this information, the force required for the shearing operation can be calculated.

$$F_s = S * t * l \ = 320 * 10^6 \ Pa * (0.009 \ m)^2 = 25.9 \ kN$$

Assuming this force is generated by exerting a torque on a simplified arm with length indicated below on Figure 20, the torque required for the shearing operation can be calculated.

$$T_s = F_s * d_s = 25.9 \ kN * 0.16 \ m \ = 4147 \ N \cdot m$$

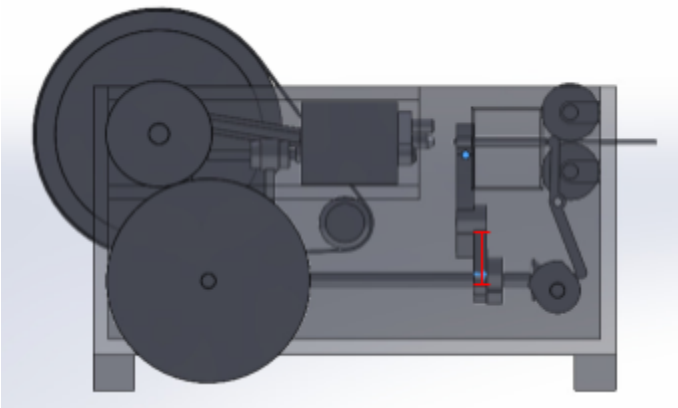

Figure 20. SolidWorks Assembly Showing Dimension for Shearing Force Moment Arm (red)

Even though the shearing operation is only a fraction of the cycle, as a conservative estimate it is assumed that the torque required to drive the accessory gearing system is constant at the maximum shearing torque. Therefore, this is the torque exerted on the longitudinal shaft, which must be transmitted through the bevel gears from the jack shaft and driving gear. Using the ratio of gear diameters, the torque of the driving pinion can be calculated knowing the torque of the driving gear.

$$\frac{d_A}{d_B} = \frac{n_B}{n_A} = \frac{T_A}{T_B}$$

$$T_p = \frac{d_p}{d_g} * T_g = \frac{408 \ mm}{784 \ mm} * 4147 \ N \cdot m = 2158 \ N \cdot m$$

This torque from the secondary accessories is transmitted along the crankshaft from the flywheel, along with the oscillating torque required for the heading operation. Therefore, the flywheel must provide torque equal to the sum of the torque loads from the accessory gearing system and from the heading operation. However, the torque calculated for the accessory gearing system was greater than the maximum torque required for the heading operation, contradicting expectations. Realistically this conclusion seems unlikely. Instead it may just be the result of an overly conservative estimate of the torque required for the accessory gearing system. The components of the gearing system and their relationships are described below in Table 2.

Part	Relationships	Diameter (mm)	Rotational Speed (RPM)	Torque (N*m)
Crankshaft	Fixed to driving pinion	N/A	350	2158
Driving Pinion	Fixed to crankshaft, meshes with driving gear	408		
Driving Gear	Meshes with driving pinion, fixed to jack shaft	784	182	4147
Jack Shaft	Fixed to driving gear and bevel that drives longitudinal shaft	Bevel outer: 164.84		
Longitudinal Shaft	Fixed to bevel driven by jack shaft	Bevel outer: 164.84		

Table 2. Analysis of Gearing System Used to Drive Accessory Operations

Crankshaft Bearing Selection

As can be seen in the free body diagram of the crankshaft (Figure 3), the crankshaft is loaded perpendicular to its axis as it rotates by the connecting rod. Therefore, the bearings that support the crankshaft will experience radial loading during heading operation. Given the high amount of stress the crankshaft is under during heading, the bearings must also be able to support significant radial loads. For this reason it is assumed that the crankshaft is supported by roller bearings instead of ball bearings, since roller bearings are better suited for supporting radial loads.

Understanding how the crankshaft is to be loaded, an appropriate set of SKF bearings is estimated that may have been used to support the crankshaft. SKF bearings use American Bearing Manufacturer Association (ABMA) standards, which include a rated life of $L_R = 10^6$ revolutions and the following Weibull parameters: $x_0 = 0.02$, $\theta = 4.459$, and $b = 1.483$.

A design load of 187.5 kN is used for each bearing since the average force from the heading operation of 375 kN is assumed to be distributed equally between the two bearings. Additionally, it is anticipated that the bearings would be designed to last for about 50 years of machine operation since many cold-forming machines are still functional decades after they were produced.

The cold forging header machine is expected to operate for 260 days a year at 60 hours a day producing 175 parts/min (350 RPM). Therefore the design life in revolutions can be calculated as follows:

$$L_d = (350\ RPM) \times \frac{60\ mins}{1\ hour} \times \frac{6\ hours}{1\ day} \times \frac{260\ days}{1\ year} \times 50\ years = 1,638 \times 10^6\ revolutions$$

Using a reliability of 90%, the dynamic load rating of a bearing that would meet the design requirements can be determined.

$$C_{10} = F_D \times (\frac{L_D}{L_R})^{1/a} \text{ where } a = \frac{10}{3} \text{ for roller bearings}$$
$$C_{10} = 187.5\ kN \times (\frac{1638*10^6}{10^6})^{3/10} = 187.5\ kN \times (1638)^{3/10} \approx 1.73 \times 10^6\ N$$

Using a recent SKF catalog, a cylindrical roller bearing that would meet the above dynamic load rating and that had a bore diameter closest to the estimated crankshaft diameter of 78.4 mm was found on page 150 with designation NJG 2334 VH.[6] The selected bearing has a dynamic load rating of $1.76 \times 10^6\ N$ and a bore diameter of 170 mm. Bearings with bore diameters in the range of the shaft diameter were not rated for the magnitude of loads the crankshaft bearings were expected to experience. Given this relatively large bore diameter, it is likely that the crankshaft actually has shoulders on either end where the bearings would be mounted. These shoulders on the crankshaft could lead to stress concentrations not considered during the initial failure analysis of the crankshaft.

A reliability of 90% for the bearings is reasonable, especially given the machine is automated so failure would not likely result in harm to humans. However, if the bearings did fail it is possible that the crankshaft or other components in the system would also fail as the angular momentum of the flywheel continued to keep the machine in operation. This could be an extremely expensive loss and may wreck the entire machine. Using the reliability of the crankshaft in fatigue failure along with the reliability of the bearings, an overall reliability of the crankshaft system can be calculated.

$$P(\textit{crankshaft system functions properly}) = R_{crankshaft} \times R_{bearing\ 1} \times R_{bearing\ 2} = 0.9^3 = 0.729$$

The reliability of the full crankshaft system is uncomfortably smaller than the 90% reliability of each bearing. If instead bearings were used with 95% reliability, the overall reliability of the crankshaft system could be brought up to a more reasonable level.

$$P(\textit{crankshaft system functions properly}) = R_{crankshaft} \times R_{bearing\ 1} \times R_{bearing\ 2} = 0.9 \times 0.95^2 \approx 0.812$$

To find bearings with this higher level of reliability, the increased dynamic load rating at which the bearings would have this reliability can be calculated using the same assumptions as before with the exception of a reliability of 95% now instead of 90%. Additionally, an application factor of 3 is added to ensure even greater reliability given the particularly high levels of impact the crankshaft bearings are expected to endure during heading operation.

$$C_{10} = a_f * F_D * \left[\frac{x_D}{x_0+(\theta-x_0)*[ln(1/R_D)]^{1/b}}\right]^{1/a} \text{ where } x_D = \frac{L_D}{L_R},\ R_D = 95\% = 0.95$$

$$C_{10} = 3 * 187.5\ kN * \left[\frac{1638}{0.02+(4.459-0.02)*[ln(1/0.95)]^{1/1.483}}\right]^{3/10} \approx 5.98 \times 10^6\ N$$

Using the same SKF catalog, a spherical roller bearing that would meet the above dynamic load rating and that had a bore diameter closest to the estimated crankshaft diameter of 78.4 mm was found on page 170 with designation 23276 CA/W33. The selected bearing has a dynamic load rating of $6.126 \times 10^6\ N$ and a bore diameter of 380 mm. Again, given this large bore diameter, it is likely that the crankshaft actually has shoulders on either end where the bearings would be mounted.

Flywheel Size and Motor Analysis

Flywheel Size Analysis

As mentioned, the crankshaft requires significant levels of torque to drive the heading operation, which only occurs over a portion of the cycle. To provide this level of energy at once, a motor with significant power would be required. However, a flywheel is capable of storing energy output from a motor as rotational energy over the entire cycle and releasing the energy quickly at the high rates necessary for the torque of the heading operations, reducing the requirements for the motor. Using the needed heading torques calculated earlier, the size and energy requirements of the flywheel can be calculated.

The flywheel and the motor belting system driving it were not detailed in the patent drawing, however the SolidWorks model assumed a diameter of 950 mm for the flywheel. Additionally, given the dimensions of the machine, the diameter of the flywheel should not exceed 1000 mm [4]. It is assumed that the diameter of the flywheel is 900 mm, $d = 0.9\ m$.

The change in energy of the flywheel over the entire heading cycle must be zero in order for the flywheel and therefore machine as a whole to operate continuously. Since all the energy needed to drive the crankshaft must come as an output from the flywheel, the motor must input that magnitude of energy to the flywheel over the course of the heading cycle. Since one heading cycle consists of two punches, each of which are a full rotation of the crankshaft, one cycle is 4π radians. Each of the preheading and final heading operations occur over $\pi/6$ radians. Therefore, the flywheel is storing energy for the remaining $1 - (\frac{2/6}{4}) = 11/12$ th of the cycle.

Using the earlier calculations in figure 10, the energy required for preheading was 425 N*m and the energy for final heading was 2025 N*m. Using this information, the overall energy output to power one heading cycle can be determined.

$$E_{out} = 425\ N \cdot m + 2025\ N \cdot m = 2450\ J$$

Therefore, the energy being stored by the motor belting system in the flywheel over the 11/12th of the heading cycle when heading isn't occurring can also be calculated.

$$\Delta E = \tfrac{11}{12} * E_{out} = \tfrac{11}{12} * 2450\ J = 2245.8\ J$$

To account for energy losses due to friction and heat dissipation that would occur in the machine during operation, the mechanical efficiency of the flywheel is assumed to be 90%. Therefore, more energy must actually be stored in the flywheel for each heading cycle than can be output to the machine operation.

$$\Delta E_{flywheel} = \frac{\Delta E}{\eta} = \frac{2245.8J}{0.9} = 2495.3J$$

Using the information tabulated below in Figure 21, the coefficient of speed fluctuation can be determined for the flywheel. The cold forging header machine falls under the category of punching, shearing, and power presses, so the coefficient of speed fluctuation ranges from 0.10 to 0.15. Due to the high level of force required for the heading operation which would lead to greater speed variation of the flywheel, the value is assumed to be on the higher end of the given range, $C_s = 0.15$.

S.No.	Type of machine or class of service	Coefficient of fluctuation of speed (C_S)
1.	Crushing machines	0.200
2.	Electrical machines	0.003
3.	Electrical machines (direct drive)	0.002
4.	Engines with belt transmission	0.030
5.	Gear wheel transmission	0.020
6.	Hammering machines	0.200
7.	Pumping machines	0.03 to 0.05
8.	Machine tools	0.030
9.	Paper making, textile and weaving machines	0.025
10.	Punching, shearing and power presses	0.10 to 0.15
11.	Spinning machinery	0.10 to 0.020
12.	Rolling mills and mining machines	0.025

Figure 21. Table of Speed Fluctuation Coefficients [7]

The average rotational speed of the flywheel is assumed to be the same as that of the crankshaft.

$$\omega_f = 350\ RPM\ * \frac{1 min}{60 s} * \frac{2\pi\ rad}{1\ rev} \approx 36.65\ rad/s$$

To size the flywheel, the moment of inertia required to store the energy necessary for heading operation must be determined. The moment of inertia can be found using the definition of kinetic energy for the flywheel, relating the flywheel energy to its moment of inertia and speed.

$$\Delta E = E_2 - E_1 = C_S * I * \omega^2$$
$$I = \frac{\Delta E}{C_S * \omega^2} = \frac{2495.3 J}{0.15 * (36.65\ rad/s)^2} \approx 12.38\ kg * m^2$$

Using the calculated moment of inertia, dimensions of the flywheel that achieve this moment of inertia can also be determined. Flywheels are typically designed with greater mass distributed radially away from the axis of rotation in order to maximize their moment of inertia

and thus rotational energy. The flywheel is assumed to have 90% of its moment of inertia in the rim.

$$I_{rim} = 0.9 * I_{total} = 0.9 * 12.38\ kg \cdot m^2 \approx 11.15\ kg \cdot m^2$$

The outer rim of the flywheel is approximated as a hoop, with a moment of inertia of $I_{rim} = m_{rim} * r^2$. Using the assumed flywheel diameter of 0.9 m and thus radius of 0.45 m, the mass located in the rim of the flywheel can be calculated.

$$m_{rim} = \frac{I_{rim}}{r^2} = \frac{11.15\ kg \cdot m^2}{(0.45\ m)^2} \approx 55\ kg$$

To translate this mass stored in the rim of the flywheel into flywheel dimensions, the flywheel is assumed to be made of grey cast iron, having density $\rho = 7100\ kg/m^3$. Grey cast iron is a common material for flywheels involved in punching operations at similar speed ranges since it is cost effective and strong [8]. The rim is assumed to have a square cross-section ($b = h$). Based on the mass of the rim of the flywheel, the dimensions of the rim cross-section are calculated.

$$m_{rim} = \rho * V_{rim} = \rho * \pi * D_{rim} * b * h$$

$$b * h = \frac{m_{rim}}{\rho * \pi * D_{rim}} = \frac{55\ kg}{(7100\ kg/m^3) * \pi * (0.9\ m)} = 0.0027\ m^2$$

$$b = h = \sqrt{0.0027\ m^2} = 0.052\ m$$

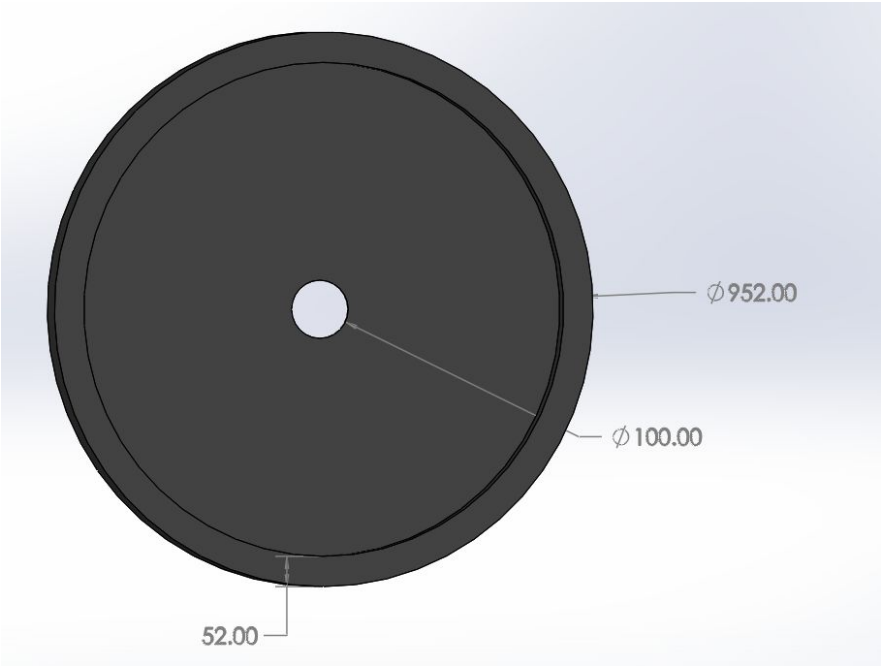

Figure 22. Model of Possible Flywheel Design (dimensions in mm)

Based on these dimensions, a basic SolidWorks model (Figure 22) was created to determine a possible distribution for the rest of the mass. Based on this model, a 3mm thick plate inside the hoop with a hole of 100 mm for the crankshaft and necessary bearings had a calculated moment of inertia of 12.28 $kg \cdot m^2$, just under the desired 12.38 $kg \cdot m^2$. However, the grey cast iron used in the SolidWorks model had a greater density than 7100 kg/m^3, so the comparison is not exact.

Flywheel-Belt-Motor Systems Analysis

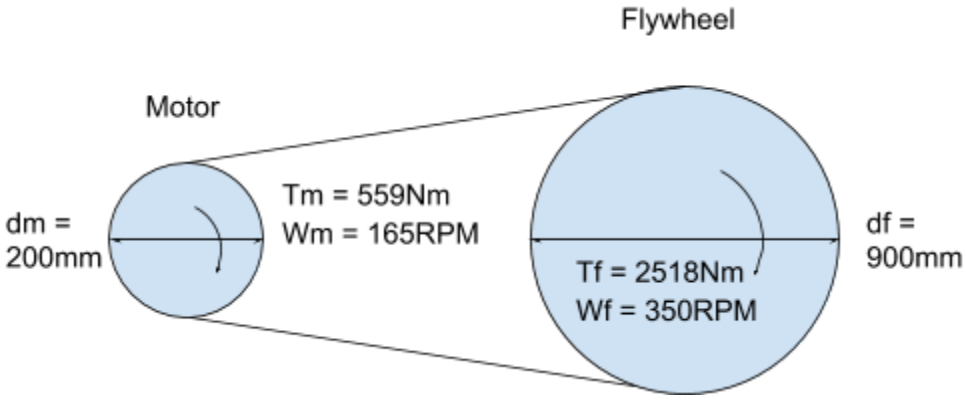

Figure 23. Diagram of Motor-Flywheel Pulley System

The flywheel is driven by a motor through a belt and pulley system. The pulley attached to the motor has a measured diameter of 200mm in SolidWorks, while the flywheel was assumed to have a diameter of 900mm. Since the motor and flywheel are connected by a belt, they must have the same linear speed. Based on the assumed rotational speed of 36.65 rad/s for the flywheel, the rotational speed of the motor can then be calculated, since $\omega_{motor} * r_{motor} = \omega_{flywheel} * r_{flywheel}$.

$$\omega_{motor} = \frac{\omega_{flywheel} * r_{flywheel}}{r_{motor}} = \frac{36.65 rad/s * 0.45m}{0.1m} = 165 rad/s$$

The force along the taut side of the belt, which is the top of the belt in Figure 23 must have a constant force throughout, so the force of the belt on the flywheel and on the motor must also be equal. As a conservative estimate, it is assumed the torque of the flywheel is the sum of the average torque for both heading operations and the torque calculated for the shearing, so the torque the flywheel exerts on the crankshaft is $T_f = 2128Nm + 322Nm + 67.6Nm = 2518Nm$. The torques on the flywheel from the belt and from the crankshaft must balance, so the torque from the belt on the flywheel is the same. By equating the force on the belt from the crankshaft with the force on the belt by the motor using $T = F * r$, the torque on the motor can be calculated.

$$\frac{T_m}{r_m} = \frac{T_f}{r_f} \text{ so } T_m = \frac{T_f}{r_f} * r_m = \frac{2518Nm}{0.45m} * 0.1m = 559Nm$$

The power provided by the motor in order to drive the flywheel with these conditions is

$$P = T_m * \omega_m = 559Nm * 165rad/s = 92.3kW$$

Therefore, the motor must rotate at a rotational speed of 165 rad/s with a torque of 559Nm and power of 92.3kW in order to drive the flywheel with enough energy for the heading operation.

References

[1] Asnafi, Nader. “On Tool Stresses in Cold Heading of Fasteners.” *Engineering Failure Analysis*, vol. 6, no. 5, 1999, pp. 321–335., doi:10.1016/s1350-6307(98)00050-8.

[2] “S7, D2, A2: Difference in Tool Steel Properties.” *Paulo*, 20 Feb. 2018, www.paulo.com/s7-d2-a2-difference-tool-steel-properties/.

[3] McNulty, Michael. "Spotlight On Cold Forming Machinery & Tooling". *Bluetoad.Com*, 2020, https://www.bluetoad.com/article/Spotlight+On+Cold+Forming+Machinery+%26+Tooling/1927446/245514/article.html.

[4] Rathod Balasaheb S, Satish. M. Rajmane. “A Case Study on Design of a Flywheel for Punching Press Operation”. International Journal of Engineering and Advanced Technology (IJEAT), vol. 3, no. 4, 2014. http://courses.me.metu.edu.tr/courses/me418/index%20_files/flywheeldesignfor%20a%20punchpress.pdf

[5] “SAE-AISI 5135 (G51350) Chromium Steel”. *MakeItFrom.com,* 2020. https://www.makeitfrom.com/material-properties/SAE-AISI-5135-G51350-Chromium-Steel

[6] “SKF Bearings and Mounted Products” https://www.skf.com/binaries/pub12/Images/0901d196807026e8-100-700_SKF_bearings_and_mounted_products_2018_tcm_12-314117.pdf

[7] Chaudhari, Keval. “Coefficient of Fluctuation of Speed”. Engineer Gallery, 11 Sept. 2015, http://www.engineersgallery.com/coefficient-of-fluctuation-of-speed/

[8] Matthews, Dave. “Flywheels 101: Choose the Best Flywheel for your Engine and Application”. On All Cylinders. 13 March 2020. https://www.onallcylinders.com/2020/03/13/flywheels-101-choose-the-best-flywheel-for-your-engine-and-application/